



Lawrence Berkeley Laboratory

UNIVERSITY OF CALIFORNIA

CHEMICAL SCIENCES DIVISION

Submitted to Physical Review B

Spectroscopic Studies and Crystal Field Analyses of Am^{3+} and Eu^{3+} in the Cubic Symmetry Site of ThO_2

S. Hubert, P. Thouvenot, and N. Edelstein

January 1993



REFERENCE COPY |
Does Not |
Circulate |

Bldg. 50 Library.

LBL-33524

Copy 1

DISCLAIMER

This document was prepared as an account of work sponsored by the United States Government. Neither the United States Government nor any agency thereof, nor The Regents of the University of California, nor any of their employees, makes any warranty, express or implied, or assumes any legal liability or responsibility for the accuracy, completeness, or usefulness of any information, apparatus, product, or process disclosed, or represents that its use would not infringe privately owned rights. Reference herein to any specific commercial product, process, or service by its trade name, trademark, manufacturer, or otherwise, does not necessarily constitute or imply its endorsement, recommendation, or favoring by the United States Government or any agency thereof, or The Regents of the University of California. The views and opinions of authors expressed herein do not necessarily state or reflect those of the United States Government or any agency thereof or The Regents of the University of California and shall not be used for advertising or product endorsement purposes.

Lawrence Berkeley Laboratory is an equal opportunity employer.

DISCLAIMER

This document was prepared as an account of work sponsored by the United States Government. While this document is believed to contain correct information, neither the United States Government nor any agency thereof, nor the Regents of the University of California, nor any of their employees, makes any warranty, express or implied, or assumes any legal responsibility for the accuracy, completeness, or usefulness of any information, apparatus, product, or process disclosed, or represents that its use would not infringe privately owned rights. Reference herein to any specific commercial product, process, or service by its trade name, trademark, manufacturer, or otherwise, does not necessarily constitute or imply its endorsement, recommendation, or favoring by the United States Government or any agency thereof, or the Regents of the University of California. The views and opinions of authors expressed herein do not necessarily state or reflect those of the United States Government or any agency thereof or the Regents of the University of California.

**Spectroscopic Studies and Crystal Field Analyses of Am³⁺ and
Eu³⁺ in the Cubic Symmetry Site of ThO₂**

S. Hubert,[†] P. Thouvenot,[†] and N. Edelstein^{*}

**[†]Laboratoire de Radiochimie, Institut de Physique Nucleaire
B.P. No. 1, 91406 Orsay (France)**

**^{*}Lawrence Berkeley Laboratory, Chemical Sciences Division,
University of California, Berkeley, California 94720 (USA)**

**This work was supported in part by the Director, Office of Energy
Research, Office of Basic Energy Sciences, Chemical Sciences Division
of the U.S. Department of Energy under Contract No. DE-AC03-
76SF00098.**



Spectroscopic Studies and Crystal Field Analyses of Am^{3+} and Eu^{3+} in the Cubic Symmetry Site of ThO_2

S. Hubert,[†] P. Thouvenot,[†] and N. Edelstein^{*}

[†]Laboratoire de Radiochimie, Institut de Physique Nucleaire, B.P. No. 1,
91406 Orsay (France)

^{*}Lawrence Berkeley Laboratory, Chemical Sciences Division, University of California,
Berkeley, California 94720 (USA)

Abstract

Fluorescence and excitation spectra of Am^{3+} diluted in ThO_2 are reported at room and liquid helium temperatures along with fluorescence data for Eu^{3+} diluted in ThO_2 . The Eu^{3+} data can be assigned primarily to magnetic dipole transitions, but the Am^{3+} data appear to be primarily phonon-assisted electric-dipole transitions. Earlier electron paramagnetic resonance (EPR) data on Pu^{3+} diluted in ThO_2 have set limits on the possible ratios of the crystal field parameters B_0^4/B_0^6 for this system. Assuming the same ratio should hold for $\text{Am}^{3+}/\text{ThO}_2$, the observed transitions were assigned and the values for the crystal field parameters $B_0^4 = -6731 \text{ cm}^{-1}$, $B_0^6 = 714 \text{ cm}^{-1}$ were obtained. The B_0^4 value is the same order of magnitude as found earlier in inelastic neutron scattering experiments for UO_2 and NpO_2 , but B_0^6 for $\text{Am}^{3+}/\text{ThO}_2$ is much smaller than determined in the neutron experiments.

Spectroscopic Studies and Crystal Field Analyses of Am^{3+} and Eu^{3+} in the Cubic Symmetry Site of ThO_2

S. Hubert,[†] P. Thouvenot,[†] and N. Edelstein^{*}

[†]Laboratoire de Radiochimie, Institut de Physique Nucleaire, B.P. No. 1,
91406 Orsay (France)

^{*}Lawrence Berkeley Laboratory, Chemical Sciences Division, University of California,
Berkeley, California 94720 (USA)

1. Introduction

Few detailed analyses of the optical spectra of trivalent americium in highly symmetric cationic sites have been published. The most complete analysis has been given by Carnall¹ for Am^{3+} in LaCl_3 and AmCl_3 ^{2,3} where the Am^{3+} ion is at a site of D_{3h} symmetry. By fitting the absorption and fluorescence data to a phenomenological Hamiltonian Carnall found very good agreement between the calculated and experimental energy levels. Chudnovskaya et al.^{4,5} have reported the absorption and fluorescence spectra of Am^{3+} in $\text{Cs}_2\text{NaLnCl}_6$, where Am^{3+} is at an O_h symmetry site. However, the crystal field analysis was carried out only for the absorption and luminescence spectra in the ground term (7F) region. In this paper, we present the experimental results and an analysis of the fluorescence and excitation spectra of the isoelectronic ions Am^{3+} ($5f^6$) and Eu^{3+} ($4f^6$) diluted in powdered samples of ThO_2 .

Thorium dioxide is an interesting host matrix for a variety of reasons. It is easy to synthesize as a powder, it crystallizes in the face centered cubic structure described by the O_h^5 space group (fluorite structure), and it is the first and simplest member (no 5f electrons) of the actinide dioxide series. Optical studies have been published on tetravalent actinides diluted in ThO_2 .^{6,7} EPR studies of Pu^{3+} in ThO_2 [8] plus optical studies of trivalent f^n ions⁹⁻¹³ in ThO_2 suggest the local symmetry remains cubic and thus make this matrix attractive for further work. Preliminary results on the luminescence properties of Am^{3+} ($5f^6$) and Eu^{3+} ($4f^6$)^{9,10} have confirmed that, at least for diluted samples, both ions are substituted into the cationic site and retain cubic symmetry. Since trivalent ions replace a 4+ ion host, the charge compensation appears to migrate far away from the dopant ions.

The heavier actinide dioxides (UO_2 , NpO_2 , PuO_2) have been the subjects of numerous studies.¹⁴⁻¹⁸ One of the major questions in these materials is the interaction of the 5f electrons of the actinide ion with their neighbors. The traditional way of

describing such a system is in terms of a single ion crystal-field Hamiltonian which, for an f^n ion in O_h symmetry, requires two crystal-field parameters. Recently, inelastic neutron scattering has been used to determine the crystal-field energy levels of the ground multiplets of UO_2 , NpO_2 , and PuO_2 , and the data were analyzed in terms of the crystal field model.^{15,17,18} Also Goodman has presented local-density molecular orbital calculations which give estimates of the crystal-field parameters in the actinide dioxides.¹⁴

In this paper, the crystal-field parameters for Am^{3+} in ThO_2 are derived from the analysis of the optical spectra. These parameters together with the previously reported EPR data of Pu^{3+} and Am^{4+} in ThO_2 and CeO_2 , provide an estimate of the crystal field for Am^{4+} in CeO_2 . CeO_2 is isostructural with the actinide dioxides, and has a lattice parameter between NpO_2 and PuO_2 . These results will be discussed and compared with earlier measurements.

2. Experimental procedure

The ThO_2 samples doped with Am^{3+} (5×10^{-2} atom%) and Eu^{3+} (0.1 atom%) were synthesized as powders according to the method described earlier.⁹ Although Kolbe et al.⁸ had measured the EPR spectrum of Am^{4+} in single crystals of Am/ThO_2 , no evidence of tetravalent americium could be found optically in our samples. If Am^{4+} exists in our samples, it might be at a much smaller concentration than for Am^{3+} . The calcination temperature used for synthesizing the Am/ThO_2 powder ($850^\circ C$) is lower than the single crystal synthesis temperature ($1350^\circ C$).⁸ The synthesis procedure could influence the final oxidation state of the Am ion.

Fluorescence spectra were recorded between room and liquid helium temperatures and analyzed with a 1m JOBIN-YVON monochromator with a dispersion of $8 \text{ \AA}/\text{mm}$. Fluorescence between 400-850 nm was detected by a photomultiplier (R 636 Hamamatsu) while fluorescence from 800 to 2400 nm was detected by a PbS photodiode. This experimental setup was controlled by a PC. The sample was placed in a liquid helium optical cryostat (OXFORD Instruments) with a regulated, heated gas system allowing the temperature to be varied between 10 and 300 K. A SOPRA nitrogen laser (length pulse 7 ns) followed by a LAMBDA-PHYSIK dye laser (pulse length 7 ns and line width 0.1 cm^{-1}) was used as the excitation source for the fluorescence and excitation spectra reported in this paper.

3. Theory and symmetry considerations

The crystal structure of thorium dioxide has each Th⁴⁺ ion at the center of a cube of oxygen ions, and each oxygen ion has about it a tetrahedron of thorium ions.¹⁹ The ThO₂ structure is isomorphic with the CaF₂ structure and has space group symmetry O_h⁵. However in the far infrared spectrum of our pure powdered sample, a slight distortion was observed.¹⁰ Weak shoulders appeared in the spectrum around 96 and 275 cm⁻¹, the FIR active mode at 356 cm⁻¹ was the most intense, but the Raman active mode at 456 cm⁻¹^{20,21} (inactive in FIR) was observed as well. Nevertheless, several experimental observations^{10,13} suggest that like tetravalent actinides,⁶ the trivalent ions Eu³⁺ and Am³⁺ diluted in the matrix are substituted into the cationic site and keep the eight-fold cubic symmetry. This means that for diluted systems using our synthesis procedure, the charge compensation vacancies migrate far away from the dopant ions.

In the case of a structure with an inversion center, the f-f electric dipole transitions are forbidden by the selection rules, while the f-f magnetic dipole transitions ($\Delta J = 1$) are allowed. Thus the excitation and fluorescence spectra have a predominantly vibronic character. In our data, the normal mode frequencies appeared to be about the same for coupling to the ground state as to the excited electronic states. The electronic energy levels deduced from the excited state vibronic structure were fit by simultaneous diagonalization of the free ion and crystal-field Hamiltonians, H_{FI} and H_{CF}, where:

$$\begin{aligned}
 H_{FI} = & \sum_{k=0,2,4,6} F^k(nf, nf) f_k + \zeta_f \alpha_{s.o.} + \alpha L(L+1) \\
 & + \beta G(G_2) + \gamma(R_7) + \sum_{\substack{k=2,8 \\ k \neq 5}} T^k t_k \\
 & + \sum_{k=0,2,4} M^k m_k + \sum_{k=2,4,6} P^k p_k
 \end{aligned}$$

and

$$\begin{aligned}
 H_{CF} = & B_0^4 [C_0^4 + (5/14)^{1/2} (C_{-4}^4 + C_4^4)] + \\
 & B_0^6 [C_0^6 - (7/2)^{1/2} (C_{-4}^6 + C_4^6)].
 \end{aligned}$$

The $F^k(nf, nf)$'s and ζ_f above represent the radial parts of the electrostatic and spin-orbit interactions, respectively, between f electrons, while f_k and $\alpha_{s.o.}$ are angular parts of these interactions. The parameters α , β , γ are associated with the two-body effective operators of the configuration interaction and the T^k are the corresponding parameters of the three-body configuration interaction operators. The M^k parameters represent the spin-spin and spin-other-orbit interactions while the P^k parameters arise from electrostatic-spin-orbit interactions with higher configurations. The crystal-field interaction for O_h symmetry is parametrized by B_0^4 and B_0^6 , and the angular operators $C_q^{(k)}$ are the usual Racah tensors.²²

Crystal-field parameters for trivalent actinides substituted for Th^{4+} ions in ThO_2 have not been evaluated. However, EPR measurements on Pu^{3+}/ThO_2 do set limits on the possible ratios of the parameters B_0^4/B_0^6 . For Pu^{3+} in cubic symmetry, the Γ_7 ($J = 5/2$) crystal-field state is the ground state. Higher-lying crystal-field states are relatively close in energy and are coupled into the ground state by the crystal field. The measured g value thus depends on the strength of the crystal field, and the relative strengths of the crystal field at the Pu^{3+} impurity site for a number of different cubic host crystals have been determined by this method.^{23,24}

The measured g value for the ground Γ_7 ($J = 5/2$) state of Pu^{3+}/ThO_2 is $|g| = 1.3124(5)$. Since Pu and Am are nearest neighbors in the Periodic Table, we expect the crystal field at a Th^{4+} cubic site to be very similar. In order to limit the possible values of the crystal-field parameters, we assume that, at least in the initial fitting procedures, the values of the Am^{3+} crystal-field parameters for Am^{3+}/ThO_2 must also fit the measured g value for Pu^{3+}/ThO_2 . Some ranges of values for the crystal-field parameters which give the measured g value for Pu^{3+} are shown in Fig. 1A. The calculated values were obtained by using all free ion energy levels below $\sim 20000 \text{ cm}^{-1}$ to calculate crystal-field matrix elements, and then diagonalizing the resulting matrices following the procedures of the Crosswhites.²⁵ The g values of the ground state were calculated from the resultant eigenvectors.

The energy levels for Am^{3+}/ThO_2 were obtained in a similar way. The free-ion energy levels up to 30000 cm^{-1} were determined using the free-ion parameters found by Carnall for $Am^{3+}/LaCl_3$. The crystal-field matrix elements were calculated with these free ion eigenvectors and these matrices were used to fit the experimental electronic levels.

4. Experimental results and analysis of the spectra

All optical spectra reported in this paper were obtained on powders. All transitions and/or states will be described by referring to either the free ion J states and/or the O_h group labels ($\Gamma_1, \Gamma_2, \Gamma_3, \Gamma_4, \Gamma_5$) for an f^n ion where n is an even number. In this notation Γ_1 and Γ_2 are singlets, Γ_3 is a doublet, Γ_4 and Γ_5 are triplets.²⁶ All crystal field states from the various J multiplets may be classified by these symmetry labels. The lowest energy Γ_N state ($N = 1-5$) will be numbered 1, the second lowest Γ_N state 2, etc. Only crystal field states of the same symmetry (but of different J) may be mixed by the crystal field potential, so the Γ_N labels remain as good quantum numbers. Since J mixing does occur and some levels contain more than one J component, the Am^{3+} states will be labeled by the largest J component and a prime will be added, i.e., J'.

4-1 Fluorescence spectra

The luminescence spectrum of Am^{3+}/ThO_2 in the visible has been already reported elsewhere^{9,10} and the observed lines primarily were assigned to transitions originating from the $^5D_{1'}$ state to the ground 7F_0 and low-lying $^7F_2'$ levels, in the region 570-620 nm ($^5D_{1'} \rightarrow ^7F_0$), 650-750 nm ($^5D_{1'} \rightarrow ^7F_1'$), and 800-850 nm ($^5D_{1'} \rightarrow ^7F_2'$) (Fig. 2a).²⁷ A weak group of lines was observed also in the range 520-560 nm corresponding to $^5L_6' \rightarrow ^7F_0'$ transitions. Among these groups the most intense transitions correspond to the $^5D_{1'} \rightarrow ^7F_1'$ and $^5D_{1'} \rightarrow ^7F_2'$. In the infrared spectrum, (Fig. 2b) only two groups of lines appear. The two lines at 8202 Å and 9350 Å are assigned to $^5D_{1'} \rightarrow ^7F_2'$ transition, while the group of lines between 1000-1150 nm is assigned as $^5D_{1'} \rightarrow ^7F_3'$. The vibronic band structure for all the groups makes possible the identification of the purely electronic (zero phonon) and phonon assisted transitions in the luminescence spectrum. From the vibronic structure, the zero phonon electric dipole transitions $^5L_6' \rightarrow ^7F_0'$, $^5D_{1'} \rightarrow ^7F_1'$ and $^5D_{1'} \rightarrow ^7F_3'$ were deduced and six Stark components $^7F_1'(\Gamma_4)$, $^7F_2'(\Gamma_5)$, $^7F_2'(\Gamma_3)$, $^7F_3'(\Gamma_4)$, $^5D_{1'}(\Gamma_4)$, and $^5L_6'(\Gamma_2)$ could be calculated respectively at 2637, 4583, 6079, 7294, 16765, and 18496 cm^{-1} . The assignment of transitions from the luminescence spectrum at low temperature is presented in Table I along with the frequencies belonging to the vibrations of the lattice. Note that the vibronic structure associated with most of the zero phonon lines (allowed or forbidden) contains all the frequencies corresponding to the complete vibrational representation of the lattice.¹⁰ The most intense zero phonon lines observed in the spectrum are attributed to the magnetic dipole transition $^5D_{1'} \rightarrow ^7F_2'$. In contrast to the other transitions, they are accompanied by weak vibronic structure. In O_h symmetry, the $^5D_{1'}$ level is not split by the crystal field, therefore the energy difference between the

narrow lines at 8202 Å and 9350 Å (see Fig. 2b) gives directly the splitting of the 7F_2 level ($\Delta E = 1496 \text{ cm}^{-1}$).

By comparison with the Am^{3+} , the luminescence spectrum of the isoelectronic lanthanide ion Eu^{3+} is straightforward.¹⁰ The magnetic dipole transition ${}^5D_0 \rightarrow {}^7F_1$ at 5903 Å is the most intense emission line observed in the spectrum¹⁰ and other narrow, weaker lines are attributed as well to magnetic dipole transitions ($\Delta J = 1$) as shown in Table II. All but one of the observed Eu^{3+} transitions can be assigned as magnetic dipole transitions; phonon-assisted transitions are not observed. For Eu^{3+} , the splitting of 7F_2 level is 651 cm^{-1} , about half the splitting of $\text{Am}^{3+}/\text{ThO}_2$.

4-2 Excitation spectra

For $\text{Am}^{3+}/\text{ThO}_2$, excitation spectra at room temperature and 4.2K were obtained in the visible region by monitoring the strongest emission line at 7118 Å or 8202 Å. Several dyes (BBQ, Coumarine 440, 460, 503, Rhod. 590) were used to obtain these spectra. Fig. 3 shows the excitation spectrum obtained at room temperature in the 5D_1 region using Rhodamine 590. As in the fluorescence spectrum, we clearly can assign the zero phonon line ${}^7F_0 \rightarrow {}^5D_1$ at 5963 Å (16765 cm^{-1}), which is accompanied by the characteristic vibronic structure on the higher energy side. The oscillator strength of this transition is very weak,^{28,29} and has only been observed once before in octahedral symmetry.^{4,5} We observe this transition at room temperature in the excitation spectrum and its inverse in the emission spectrum. Unfortunately, at low temperature (below 50K), the fluorescence intensity is bleached by traps which may be caused by defects due to oxygen vacancies, so clean excitation spectrum could not be obtained in this wavelength region. Excitation spectra were recorded at room and liquid helium temperatures in the following regions: 365-400 nm, 425-465 nm, 440-480 nm, 460-500 nm, 475-555 nm and 517-582 nm. The excitation spectra at low temperature are shown in Fig. 4. Vibronic features are clearly observed in the 5D_1 region and can be recognized in other spectral regions where the excited states are rather isolated. Such is the case for the lowest and the highest energy components of 5L_6 states between 515-560 nm and 480-490 nm, as well as in the region of the 5D_2 and 5G_4 levels between 440-480 nm. Among all the transitions observed in the excitation spectra, the only zero phonon line which appears corresponds to the magnetic dipole transition ($\Delta J = 1$) ${}^7F_0 \rightarrow {}^5D_1$ at 5963 Å. Note, however, that for the lowest energy component of the 5L_6 , the zero phonon line centered between the two vibronic features (see Fig. 5) appears weakly at room temperature. When the temperature is decreased, the low energy side of the vibronic structure disappears as expected.

From an analysis of the vibronic structure, the energies of some zero phonon lines were identified. Table III lists the energies of 13 Stark components, and the vibronic lines associated with them. Similar to the transitions observed in the fluorescence spectrum (Table II), the vibronic structure associated with the electronic transitions contains primarily the same phonon frequencies 96, 276, 456, and 575 cm^{-1} observed in the far infrared spectrum.¹⁰ Assignments of the $\text{Am}^{3+}/\text{ThO}_2$ levels are derived from the fluorescence and excitation measurements.

By contrast with Am^{3+} , the excitation spectrum of Eu^{3+} in the cubic site is very simple. No phonon assisted transitions are observed, and only one narrow line at 5255 Å corresponding to the magnetic dipole transition ${}^7\text{F}_0 \rightarrow {}^5\text{D}_1$ is observed at low temperature (Fig. 6).

5. Discussion

The levels were fit by simultaneous diagonalization of the free ion and crystal-field Hamiltonians as given earlier. For $\text{Am}^{3+}/\text{ThO}_2$ the $\text{Am}^{3+}/\text{LaCl}_3$ free-ion parameters were used as initial guesses along with a series of values of B_0^4 and B_0^6 which were chosen to give the experimental ground state g value for $\text{Pu}^{3+}/\text{ThO}_2$. Initially the crystal-field parameters were held fixed and only F^2 , F^4 , F^6 , and ζ were varied. After the "best" values of B_0^4 and B_0^6 were determined, further high-energy levels were assigned, and the above free-ion and crystal-field parameters were varied simultaneously. In the final iterations, the parameter α was varied also. For $\text{Eu}^{3+}/\text{ThO}_2$, the free-ion parameters (except for ζ) were fixed at the values obtained from analysis of the fluorescence data of $\text{Eu}^{3+}/\text{LuPO}_4$;³⁰ ζ and the crystal field parameters B_0^4 and B_0^6 were allowed to vary. The results of the fits and the final assignments of the experimental levels are given in Table IV for $\text{Am}^{3+}/\text{ThO}_2$ and in Table V for $\text{Eu}^{3+}/\text{ThO}_2$. The parameters are given in Table VI. O_h symmetry labels were assigned on the basis of the calculated energy levels and wavefunctions.

As expected the crystal-field parameters of $\text{Am}^{3+}/\text{ThO}_2$ are appreciably larger than for $\text{Eu}^{3+}/\text{ThO}_2$. Although we have observed only a very limited number of Am^{3+} multiplets, the free ion parameters F^2 , F^4 , F^6 , and ζ appear to be smaller than those found by Carnall for $\text{Am}^{3+}/\text{LaCl}_3$.¹ The value of the parameter α is larger than that used by Carnall but the large error associated with this parameter in our work suggests this comparison is not meaningful. The values of the crystal-field parameters seem reasonable in that we are able to get a good fit for $\text{Am}^{3+}/\text{ThO}_2$ with crystal-field parameters which also give reasonable agreement with the measured g value for $\text{Pu}^{3+}/\text{ThO}_2$.

The results for $\text{Am}^{3+}/\text{ThO}_2$ allow a re-examination of the EPR data for $\text{Pu}^{3+}/\text{ThO}_2$, $\text{Am}^{4+}/\text{ThO}_2$ and $\text{Am}^{4+}/\text{CeO}_2$. We expect the crystal-field splittings for the tetravalent ion Am^{4+} to be larger than for the isoelectronic ion Pu^{3+} . In addition, if we compare the crystal fields for Am^{4+} in the host crystal ThO_2 ($a_0 = 5.597\text{\AA}$) and CeO_2 ($a_0 = 5.41\text{\AA}$), we would expect a larger crystal field in CeO_2 than in ThO_2 because of the larger lattice constant in ThO_2 .^{31,32} This is exactly what is observed in the EPR spectra of $\text{Am}^{4+}/\text{ThO}_2$ and $\text{Am}^{4+}/\text{CeO}_2$ where the ground state g value of Am^{4+} is larger in CeO_2 (absolute magnitude) due to increased mixing of higher energy states by the larger crystal field. The calculated g values of Am^{4+} for various ranges of B_0^4 and B_0^6 are shown in Figure 1B.

We assume the minimum value of B_0^4 for Am^{4+} in ThO_2 or CeO_2 is equal to that found for Am^{3+} in ThO_2 . From Figure 1B this assumption would put the value of B_0^6 for $\text{Am}^{4+}/\text{ThO}_2$ at $\sim 800\text{ cm}^{-1}$. Increasing the value of B_0^4 decreases B_0^6 . If we make the same assumption for $\text{Am}^{4+}/\text{CeO}_2$, we get the values of $B_0^4 \cong -6700\text{ cm}^{-1}$, $B_0^6 \cong 1000\text{ cm}^{-1}$. Again as B_0^4 get larger, B_0^6 must decrease in order to get the observed g value.

Now the lattice parameter of CeO_2 is between that of NpO_2 ($a_0 = 5.425\text{\AA}$) and PuO_2 ($a_0 = 5.396\text{\AA}$).³¹ From the inelastic neutron scattering data for UO_2 the values of $B_0^4 = -7937\text{ cm}^{-1}$, $B_0^6 = 3420\text{ cm}^{-1}$ were obtained.¹⁸ The value of B_0^4 found in the neutron scattering data is within 20% of the value we have obtained with Am^{3+} as probe of the crystal field of ThO_2 , but the B_0^6 found for UO_2 is inconsistent with the optical and EPR data of $\text{Am}^{3+}/\text{ThO}_2$, $\text{Pu}^{3+}/\text{ThO}_2$ and $\text{Am}^{4+}/\text{ThO}_2$, CeO_2 .

UO_2 is a magnetic material and the U^{4+} ion has a greater radial extent than Am^{4+} . Our experiments use a paramagnetic probe in a diamagnetic host which is isostructural with UO_2 . Covalency effects in UO_2 could play a role which might affect our arguments about the magnitudes of the crystal field parameters. However the good agreement found for the UO_2 inelastic neutron scattering value of B_0^4 with our Am^{3+} B_0^4 value suggests the comparison is valid. Our results also disagree with the magnitude of the crystal field obtained by Goodman in his calculations,¹⁴ where he has found values of B_0^4 and B_0^6 of the same magnitude (but opposite sign) for UO_2 , PuO_2 , and CmO_2 .

The crystal field strength parameter N'_v ³³ provides a useful means for comparing crystal field effects on a series of f^n ions in the same matrix or the effects of different matrices with the same ion. Following Auzel, N'_v is defined as follows:

$$N'_v = [\sum_{k,q} (B_q^k)^2 / 2k + 1]^{1/2}.$$

Values of N'_v for trivalent actinide ($5f^{nN}$) ions with their counterpart ($4f^{nN}$) lanthanide ions in different host matrices are given in Table VII.

Comparison of the N'_v parameter with chloride coordination (D_{3h} for LaCl_3 , and O_h for AmCl_6^{3-}) shows the octahedral site provides a crystal field about twice as large as that of the D_{3h} site. The N'_v parameters for Am^{3+} or Eu^{3+} in ThO_2 when compared with these same ions in the elpasolite host are about twice as large. The larger crystal field found in ThO_2 is consistent with the shorter actinide-ligand distance [Th-O 2.42 Å, Am-Cl 2.54 Å]. We also report N'_v parameters for other 5f and 4f ion pairs (f^3 and f^5 configurations) in Table VII.^{34,35} The strength of the crystal field interaction is between 2 and 2.4 times larger for the trivalent actinide than for its counterpart lanthanide ion. This ratio can be used as a qualitative test of the validity of the crystal field parameters. In ThO_2 , we find the same ratio of $N'_v(5f^n)/N'_v(4f^n)$ as in LaCl_3 . Furthermore this value is consistent with the splitting of the 7F_2 level found for Am^{3+} (1496 cm^{-1}) which is 2.3 times greater than for Eu^{3+} (646 cm^{-1}).

Conclusion

The fluorescence and excitation spectra of $\text{Am}^{3+}/\text{ThO}_2$ and the fluorescence spectra of $\text{Eu}^{3+}/\text{ThO}_2$ have been assigned. The crystal field splittings of Am^{3+} in this crystal is approximately double that of its lanthanide analog consistent with other actinide/lanthanide pairs. The fourth order crystal field parameter B_0^4 is of the same magnitude as found for UO_2 and NpO_2 by inelastic neutron scattering experiments, but the sixth order parameter is appreciably smaller than that found in the neutron experiments.

Acknowledgement

This work was supported in part by the Director, Office of Energy Research, Office of Basic Energy Sciences, Chemical Sciences Division of the U.S. Department of Energy under Contract No. DE-AC03-76SF00098.

References

1. W. T. Carnall, J. Less Com. Met. 156, 221 (1989).
2. R. G. Pappalardo, W. T. Carnall and P. R. Fields, J. Chem. Phys. 51, 1182 (1969).
3. J. G. Conway, J. Chem. Phys. 40, 2504 (1964).

4. G. P. Chudnovskaya, Yu. I. Gavrish, and Yu. A. Barbanel, *Radiokhimiya* 30, 46 (1988).
5. G. P. Chudnovskaya, R. B. Dushin, V. V. Kolin, and Yu. A. Barbanel 27, 545 (1985).
6. J. B. Gruber and E. R. Menzel, *J. Chem. Phys.* 50, 3772 (1969).
7. Z. Gajek, M.P. LaHalle, J.C. Krupa, and J. Mulak, *J. Less-Common Met.* 139, 351 (1988).
8. W. Kolbe, N. Edelstein, C. B. Finch and M. M. Abraham, *Chem. Phys.* 60, 607 (1974).
9. S. Hubert and P. Thouvenot, *J. Alloys. Comp.* 180, 193 (1992).
10. S. Hubert and P. Thouvenot, *J. Lum.* 54, 103 (1992).
11. R. C. Linares, *J. Opt. Soc. Am.* 56, 107 (1966).
12. M. Breysse and L. Faure, *J. Lum.* 26, 107 (1981).
13. L. C. Porter and J. C. Wright, *J. Lum.* 27, 237 (1982).
14. G.L. Goodman, *J. of Alloys and Compounds* 181, 33 (1992).
15. J.M. Fournier, A. Blaise, G. Amoretti, R. Caciuffo, J. Larroque, M.T. Hutchings, R. Osborn, and A.D. Taylor, *Phys. Rev. B* 43, 1142 (1991).
16. J.C. Krupa and Z. Gajek, *Eur. J. Solid State Inorg. Chem.* 28, 143 (1991).
17. S. Kern, C.-K. Loong, G.L. Goodman, B. Cort, and G.H. Lander, *J. Phys. Condens. Matter* 2, 1933 (1990).
18. G. Amoretti, A. Blaise, R. Caciuffo, J.M. Fournier, M.T. Hutchings, R. Osborn, and A.D. Taylor, *Phys. Rev. B* 40, 1856 (1989).
19. R.W.G. Wyckoff, "Crystal Structures" (Interscience, New York, 1963), 2nd Ed. Vol. 1.
20. V. G. Keramidas, W. B. White, *J. Chem. Phys.* 59, 156 (1973).
21. G. M. Begun, R. G. Haire, W. R. Wilmarth, J. R. Peterson, *J. Less.Com. Met.* 162, 129 (1990).
22. W.T. Carnall, H. Crosswhite, H.M. Crosswhite, J.P. Hessler, N.M. Edelstein, J.G. Conway, G.V. Shalimoff and R. Sarup, *J. Chem. Phys.* 72, 5089 (1980).
23. N. Edelstein, H.F. Mollet, W.C. Easley, and R.J. Mehlhorn, *J. Chem. Phys.* 51, 3281 (1969).
24. D.J. Lam and S.-K. Chan, *Phys. Rev. B* 6, 307 (1972).
25. H.M. Crosswhite and H. Crosswhite, *J. Opt. Soc. Am. B* 1, 246 (1984).
26. G.F. Koster, J.O. Dimmock, R.G. Wheeler, and H. Statz, "Properties of the Thirty-Two Point Groups," (MIT Press, Cambridge, MA, 1963).

27. For an f^6 configuration, there are three 5D states. In the notation of Nielson and Koster, the lowest 5D state from which strong fluorescence occurs is labelled 5D_3 . In the text of this paper and in the figures we use the notation 5D for the 5D_3 state. The tables list the states with the Nielson and Koster classification for the f^6 LS states. C.W. Nielson and G.F. Koster, "Spectroscopic Coefficients for the p^n , d^n , and f^n Configurations," MIT Press, Cambridge, MA, 1963.
28. W. T. Carnall and B. G. Wybourne, *J. Chem. Phys.* **40**, 3428 (1964).
29. W. T. Carnall, P. R. Fields, B. G. Wybourne, *J. Chem. Phys.* **41**, 2195 (1964).
30. N. Edelstein and D. Piehler, unpublished results.
31. J.J. Katz, L.R. Morss, and G.T. Seaborg, in "The Chemistry of the Actinide Elements," 2nd Ed. J.J. Katz, G.T. Seaborg, and L.R. Morss, Eds., (Chapman and Hall, London, 1986), Vol. 2, p. 1156.
32. J.D.H. Donnay and H.M. Ondik, "Crystal Data, Vol. II: Inorganic Compounds", (National Bureau of Standards, Washington, DC, 1973), 3rd Ed., p. C-104.
33. F. Auzel and O.L. Malta, *J. Phys.* **44**, 201 (1983).
34. W.T. Carnall, H. Crosswhite, H.M. Crosswhite, "Energy Level Structure and Transition Probabilities of the Trivalent Lanthanides in LaF_3 ," Special Rep. 1977 (Chemistry Division, Argonne National Laboratory, Argonne, IL).
35. W.T. Carnall, *J. Chem. Phys.* **96**, 8713 (1992).

Table 1. Zero Phonon and Phonon Assisted Transitions
Energies from the Luminescence Spectrum at Low Temperature
(Notation from Nielson and Koster)²⁷

Wavelength $\lambda(\text{\AA})$	Wavenumber $\nu(\text{cm}^{-1})_{\text{vac}}$	Assignment ^a	ΔE
(5402)	(18506)	$^5L_6 \rightarrow ^7F_0 (3\Gamma_2 \rightarrow 1\Gamma_1)$	0
5429	18414		93
5486	18223		283
5540	18045		461
5575	17932		574
5929	16861		93
5961	16771	$^5D_3 \rightarrow ^7F_0 (7\Gamma_4 \rightarrow 1\Gamma_1)$	0
5995	16676		92
6065	16483		285
6091	16413		355
6129	16308		460
6173	16195		573
7024	14232		97
7072.5	14135	$^5D_3 \rightarrow ^7F_1 (7\Gamma_4 \rightarrow 1\Gamma_4)$	0
7118	14044		92
7214	13857		274
7309	13677		459
7373	13559		575
8202	12189	$^5D_3 \rightarrow ^7F_2 (7\Gamma_4 \rightarrow 1\Gamma_5)$	0
8269	12089		99
8397	11905		283
9350	10692	$^5D_3 \rightarrow ^7F_2 (7\Gamma_4 \rightarrow 1\Gamma_3)$	0
10249	9754		277
10447	9569		93
(10549)	(9477)	$^5D_3 \rightarrow ^7F_3 (7\Gamma_4 \rightarrow 2\Gamma_4)$	0
10653	9384		93
10877	9191		286
10957	9124		353

^aSee Table IV for a tabulation of the Am^{3+} states.

Table II. Magnetic Dipole Transitions Energies of $\text{Eu}^{3+}/\text{ThO}_2$
From the Emission Spectrum at 10K²⁷

Wavelength $\lambda(\text{\AA})$	Wavenumber $\nu(\text{cm}^{-1})_{\text{vac}}$	Assignments ^a
5903	16936	${}^5\text{D}_{30} \rightarrow {}^7\text{F}_1 (4\Gamma_1 \rightarrow 1\Gamma_4)$
5680.5	17600	${}^5\text{D}_{31} \rightarrow {}^7\text{F}_2 (7\Gamma_4 \rightarrow 1\Gamma_3)$
5477.5	18251	${}^5\text{D}_{31} \rightarrow {}^7\text{F}_2 (7\Gamma_4 \rightarrow 1\Gamma_5)$
5258.5	19012	${}^5\text{D}_{31} \rightarrow {}^7\text{F}_0 (7\Gamma_4 \rightarrow 1\Gamma_1)$
5188	19270	${}^5\text{D}_{32} \rightarrow {}^7\text{F}_3 (5\Gamma_3 \rightarrow 1\Gamma_2)^{\text{b}}$
5158	19382	${}^5\text{D}_{32} \rightarrow {}^7\text{F}_3 (5\Gamma_3 \rightarrow 2\Gamma_5)$
5121.5	19520	${}^5\text{D}_{32} \rightarrow {}^7\text{F}_3 (5\Gamma_3 \rightarrow 2\Gamma_4)$
4751	21042	${}^5\text{D}_{33} \rightarrow {}^7\text{F}_4 (3\Gamma_2 \rightarrow 3\Gamma_5)$
4737.5	21102	${}^5\text{D}_{32} \rightarrow {}^7\text{F}_1 (5\Gamma_3 \rightarrow 1\Gamma_4)$
4719	21185	${}^5\text{L}_6 \rightarrow {}^7\text{F}_4 (4\Gamma_2 \rightarrow 4\Gamma_5)$
4678.5	21368	${}^5\text{D}_{33} \rightarrow {}^7\text{F}_4 (8\Gamma_5 \rightarrow 2\Gamma_3)$
4663.5	21437	${}^5\text{D}_{33} \rightarrow {}^7\text{F}_4 (8\Gamma_4 \rightarrow 2\Gamma_3)$
4517.5	22130	${}^5\text{L}_6 \rightarrow {}^7\text{F}_4 (10\Gamma_5 \rightarrow 2\Gamma_3)$
4466.5	22383	${}^5\text{D}_{33} \rightarrow {}^7\text{F}_3 (8\Gamma_4 \rightarrow 2\Gamma_5)$

^aSee Table V for a tabulation of the Eu^{3+} states.

^bNot an allowed magnetic dipole transition.

Table III. Energies of Zero-Phonon and Phonon-Assisted Lines
From Excitation Spectra at Low Temperature

Wavelength $\lambda(\text{\AA})$	Wavenumbers $\nu(\text{cm}^{-1})$ in vacuum	$\Delta\nu$ (phonons)
5963	16765	0
5929	16861	96
5865	17045	280
5805	17221	456
5765	17341	576
5405	18496	0
5378	18589	93
5325	18774	278
5275	18952	456
5242	19072	576
5214	19174	0
5188	19270	96
5139	19453	279
5119	19530	356
5091	19637	465
5063	19746	572
5116	19541	0
5091	19637	96
5045	19817	276
5029	19879	333
4999	19998	449
4971	20111	570

Table III continued on next page.

Table III (continued)

Wavelength $\lambda(\text{\AA})$	Wavenumbers $\nu(\text{cm}^{-1})$ in vacuum	$\Delta\nu$ (phonons)
5060	19757	0
5036	19851	94
4990	20034	277
4971	20111	354
4944	20221	464
4916	20336	579
4950	20196	0
4927	20291	95
4883	20473	277
4874	20515	319
4837	20668	464
4815	20763	567
4776	20932	0
4754	21029	97
4715	21203	271
4674	21389	457
4649	21504	572
4661	21448	0
4640	21546	98
4602	21724	276
4563	21909	461
4540	22020	572
4493	22251	0
4474	22345	94
4437	22531	280
4404	22702	451
4379	22830	579

Table III (continued on next page)

Table III (continued)

Wavelength $\lambda(\text{\AA})$	Wavenumbers $\nu(\text{cm}^{-1})$ in vacuum	$\Delta\nu$ (phonons)
4396	22740	0
4377	22840	100
4344	23014	274
4309	23201	461
4361	22924	0
4344	23014	90
4308	23206	282
4295	23276	356
4275	23385	461
3947	25328	0
3922	25425	97
3904	25607	279
3877	25786	458
3861	25893	565
3840	26034	0
3826	26126	92
3800	26308	274
3788	26392	358
3773	26497	463
3762	26574	540

Table IV. Calculated and Experimental Energy Levels for $\text{Am}^{3+}/\text{ThO}_2$
(Notation from Nielson and Koster²⁷)

Level	Largest S-L-J Comp.	Calc. Energy	Exp. Energy	$\Delta(E_{\text{exp}}-E_{\text{calc}})$
$1\Gamma_1$	7F_0	4.2	0	-4.2
$1\Gamma_4$	7F_1	2655.6	2637	-18.6
$1\Gamma_5$	7F_2	4559.3	4583	23.7
$1\Gamma_3$	7F_2	6053.8	6079	25.2
$2\Gamma_4$	7F_3	7318.4	7294	-24.4
$2\Gamma_5$	7F_3	7703.9		
$1\Gamma_2$	7F_3	7960.3		
$2\Gamma_1$	7F_4	8225.1		
$3\Gamma_4$	7F_4	9230.6		
$2\Gamma_3$	7F_4	9645.6		
$3\Gamma_5$	7F_4	10288.4		
$4\Gamma_5$	7F_5	10511.5		
$4\Gamma_4$	7F_5	10734.8		
$3\Gamma_3$	7F_5	11686.6		
$5\Gamma_4$	7F_5	11757.3		
$3\Gamma_1$	7F_0	12006.9		
$4\Gamma_1$	7F_6	12381.7		
$6\Gamma_4$	7F_6	12579.8		
$5\Gamma_5$	7F_6	12730.8		
$2\Gamma_2$	7F_6	12822.0		
$4\Gamma_3$	7F_6	13035.6		
$6\Gamma_5$	7F_6	13046.7		
$7\Gamma_4$	${}^5D_{3_1}$	16767.3	16765	-2.4

Table IV (continued on next page)

Table IV (continued)

Level	Largest S-L-J Comp.	Calc. Energy	Exp. Energy	$\Delta(E_{\text{exp}}-E_{\text{calc}})$
3 Γ_2	⁵ L ₆	18537.1	18496	-41.2
7 Γ_5	⁵ L ₆	18635.6		
5 Γ_3	⁵ L ₆	18677.5		
8 Γ_5	⁵ L ₆	19114.0	19174	60.1
8 Γ_4	⁵ L ₆	19470.7	19541	70.3
5 Γ_1	⁵ L ₆	19831.6	19757	-74.6
6 Γ_3	⁵ D ₃₂	20195.9	20196	0.1
9 Γ_5	⁵ G ₁₂	20907.7	20932	24.3
4 Γ_2	⁵ G ₁₃	21289.5		
10 Γ_5	⁵ D ₃₂	21366.4		
7 Γ_3	⁵ G ₁₂	21482.4	21448	-34.4
11 Γ_5	⁵ G ₁₃	21747.6		
9 Γ_4	⁵ G ₁₃	22019.5		
12 Γ_5	⁵ H ₂₄	22266.2	22251	-15.2
10 Γ_4	⁵ H ₂₅	22311.0		
8 Γ_3	⁵ H ₂₅	22336.7		
11 Γ_4	⁵ H ₂₅	22664.8		
13 Γ_5	⁵ L ₇	22893.1		
12 Γ_4	⁵ L ₇	22899.1		
6 Γ_1	⁵ H ₂₄	22928.5	22924	-4.5
5 Γ_2	⁵ L ₇	22952.2		
9 Γ_3	⁵ H ₂₄	23180.9		
13 Γ_4	⁵ H ₂₅	23212.1		
14 Γ_5	⁵ L ₆	23320.1		

Table IV (continued on next page)

Table IV (continued)

Level	Largest S-L-J Comp.	Calc. Energy	Exp. Energy	$\Delta(E_{\text{exp}} - E_{\text{calc}})$
15 Γ_5	5L_7	23441.5		
10 Γ_3	$^5H_{24}$	23564.3		
16 Γ_5	$^5D_{33}$	23999.8		
6 Γ_2	$^5D_{33}$	24025.5		
14 Γ_4	5L_7	24055.4		
17 Γ_5	5L_6	24513.1		
11 Γ_3	5L_6	24606.9		
15 Γ_4	$^5D_{33}$	24663.4		
18 Γ_5	5L_6	24922.4		
7 Γ_1	5L_8	24973.0		
16 Γ_4	5L_6	24982.8		
12 Γ_3	5L_8	25100.1		
8 Γ_1	5L_6	25101.2		
17 Γ_4	$^5D_{33}$	25214.6		
7 Γ_2	$^5D_{33}$	25319.0	25328	9.0
19 Γ_5	$^5G_{24}$	25493.9		
18 Γ_4	$^5G_{25}$	25979.2		
13 Γ_3	$^5G_{25}$	26027.3	26034	6.7
20 Γ_5	$^5G_{25}$	26087.8		
14 Γ_3	$^5G_{32}$	26183.5		
19 Γ_4	5L_8	26252.3		
9 Γ_1	$^5G_{24}$	26498.5		

Table V. Calculated and Experimental Energy Levels for $\text{Eu}^{3+}/\text{ThO}_2$
 (Notation from Nielson and Koster²⁷)

Level	Largest S-L-J Comp.	Calc. Energy	Exp. Energy	$\Delta(E_{\text{exp}} - E_{\text{calc}})$
$1\Gamma_1$	7F_0	-20.1	0	20.1
$1\Gamma_4$	7F_1	325.6	310	-15.6
$1\Gamma_5$	7F_2	748.0	763	15.0
$1\Gamma_3$	7F_2	1383.5	1414	30.5
$2\Gamma_4$	7F_3	1886.8	1893	6.2
$2\Gamma_5$	7F_3	2059.0	2031	-28.0
$1\Gamma_2$	7F_3	2164.1	2143	-21.1
$2\Gamma_1$	7F_4	2492.1		
$3\Gamma_4$	7F_4	2816.7	2830	13.3
$2\Gamma_3$	7F_4	2986.6	2993	6.4
$3\Gamma_5$	7F_4	3287.3	3300	12.7
$4\Gamma_5$	7F_5	3749.0		
$4\Gamma_4$	7F_5	3811.0		
$3\Gamma_3$	7F_5	4208.4		
$5\Gamma_4$	7F_5	4244.3		
$3\Gamma_1$	7F_6	4909.5		
$6\Gamma_4$	7F_6	5022.7		
$5\Gamma_5$	7F_6	5121.6		
$2\Gamma_2$	7F_6	5293.2		
$6\Gamma_5$	7F_6	5372.7		
$4\Gamma_3$	7F_6	5390.2		
$4\Gamma_1$	5D_3_0	17245.2	17245	-0.2
$7\Gamma_4$	5D_3_1	19020.3	19012	-8.3

Table V (continued on next page)

Table V (continued)

Level	Largest S-L-J Comp.	Calc. Energy	Exp. Energy	$\Delta(E_{\text{exp}} - E_{\text{calc}})$
$5\Gamma_3$	$^5D_{3_2}$	21441.1		
$7\Gamma_5$	$^5D_{3_2}$	21551.7		
$3\Gamma_2$	$^5D_{3_3}$	24358.4	24342	-16.4
$8\Gamma_5$	$^5D_{3_3}$	24370.5	24361	-9.5
$8\Gamma_4$	$^5D_{3_3}$	24417.7	24430	12.3
$6\Gamma_3$	5L_6	24429.5		
$9\Gamma_5$	5L_6	24450.3		
$4\Gamma_2$	5L_6	24494.5	24485	-9.5
$10\Gamma_5$	5L_6	25132.8	25123	-9.8
$9\Gamma_4$	5L_6	25240.6		
$5\Gamma_1$	5L_6	25377.0		

Table VI. Spectroscopic Parameters^a

Parameters cm ⁻¹	Eu ³⁺ /ThO ₂ ^b	Am ³⁺ /ThO ₂ ^c
F ²	[80335.2]	48038.0(140.2)
F ⁴	[58953.9]	39684.2(212.9)
F ⁶	[41636.6]	29514.1(171.4)
ζ	1337.3(7.1)	2511.1(27.0)
α	[16.8]	33.2(8.6)
β	[-640]	[-660]
γ	[1750]	[1000]
T ²	[370]	[200]
T ³	[40]	[50]
T ⁴	[40]	[40]
T ⁶	[-330]	[-360]
T ⁷	[380]	[390]
T ⁸	[370]	[340]
M ⁰	[2.38]	[0.99]
M ²	[1.33]	[0.55]
M ⁴	[0.90]	[0.38]
P ²	[245]	[850]
P ⁴	[183.8]	[637.5]
P ⁶	[122.5]	[425]
B ₀ ⁴	-2780.2(32.2)	-6731.3(96.0)
B ₀ ⁶	266.0(26.3)	713.6(115.0)

^aAll parameters values in [] held fixed in the fitting procedure.

^b17 exp. levels, rms dev. 18.0 cm⁻¹.

^c17 exp. levels, rms dev. 47.3 cm⁻¹.

Table VII - N'_v parameters

Ion	$\text{Am}^{3+}(\text{Eu}^3)$	$\text{Am}^{3+}(\text{Eu}^3)$	$\text{Am}^{3+}(\text{Eu}^3)$	$\text{U}^{3+}(\text{Nd}^{3+})$	$\text{Pu}^{3+}(\text{Sm}^3)$
Host	ThO_2	MCl_6^{3-}	LaCl_3	LcCl_3	LaCl_3
Symmetry	O_h	O_h	D_{3h}	D_{3h}	D_{3h}
Reference	This work	[4]	[1][32]	[32,33]	[32,33]
N'_v	2945(1212)	1165(618)	648(294)	605(302)	594(249)
$\frac{N'_v(5f^n)}{N'_v(4f^n)}$	2.4	1.9	2.2	2	2.4

Figure Captions

- Figure 1. Calculated g values as a function of the crystal field parameters for O_h symmetry; A: ground state of Pu^{3+}/ThO_2 ; B: ground state of Am^{4+}/ThO_2 or Am^{4+}/CeO_2 . The horizontal lines represent the measured g values.
- Figure 2. Emission spectra of Am^{3+}/ThO_2 ; A: Visible region at room temperature; B: Visible region at 10K; C: Infra-red region at room temperature.
- Figure 3. Am^{3+}/ThO_2 excitation spectrum at room temperature, the ${}^7F_0 \rightarrow {}^5D_1$ transition.²⁷
- Figure 4. Excitation spectra of Am^{3+}/ThO_2 at 10 K. The fluorescence is measured at 712 nm.
- Figure 5. Excitation spectra of the ${}^7F_0 \rightarrow {}^5L_6$ transition at room temperature and 4.2K.
- Figure 6. Excitation spectrum of Eu^{3+}/ThO_2 at 10 K.

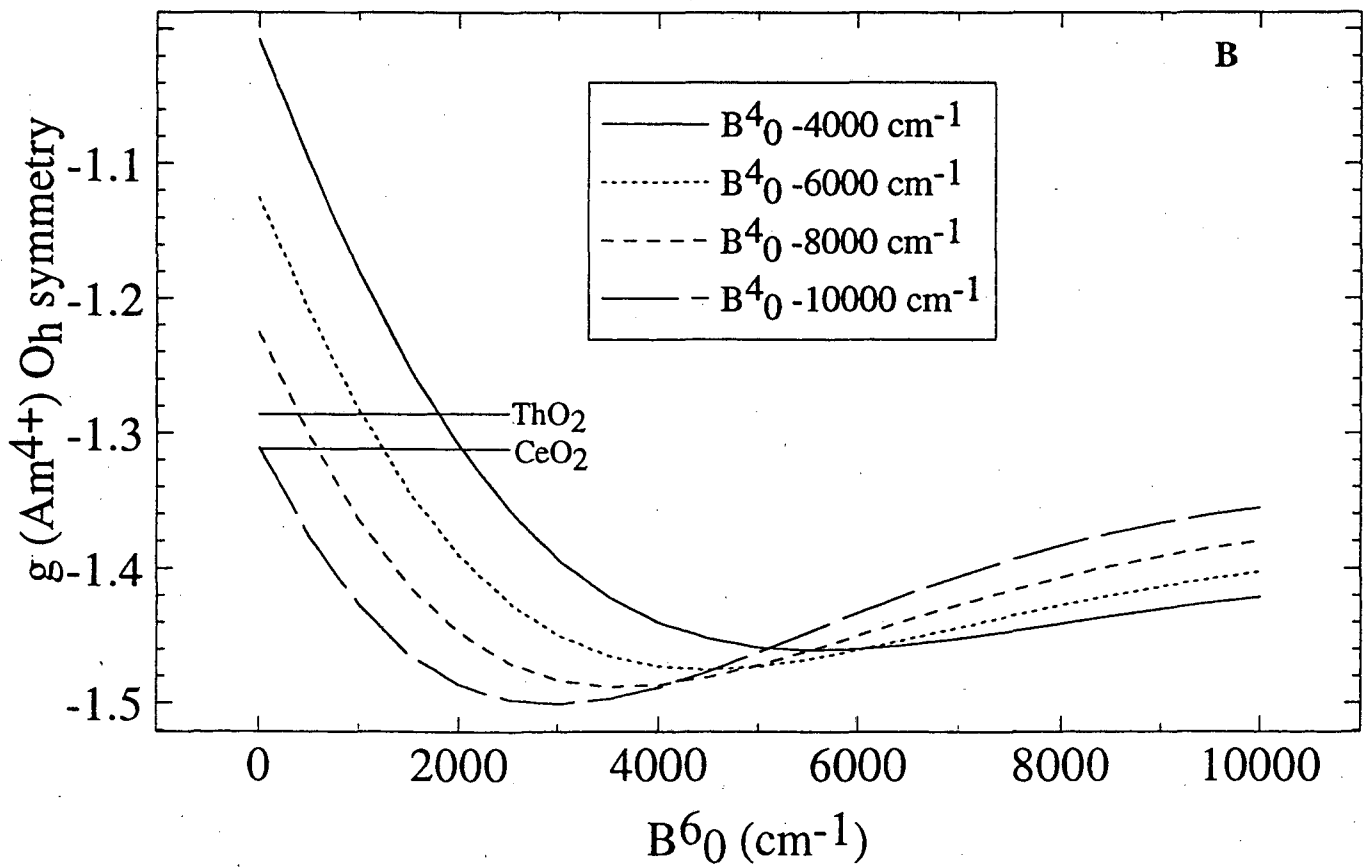
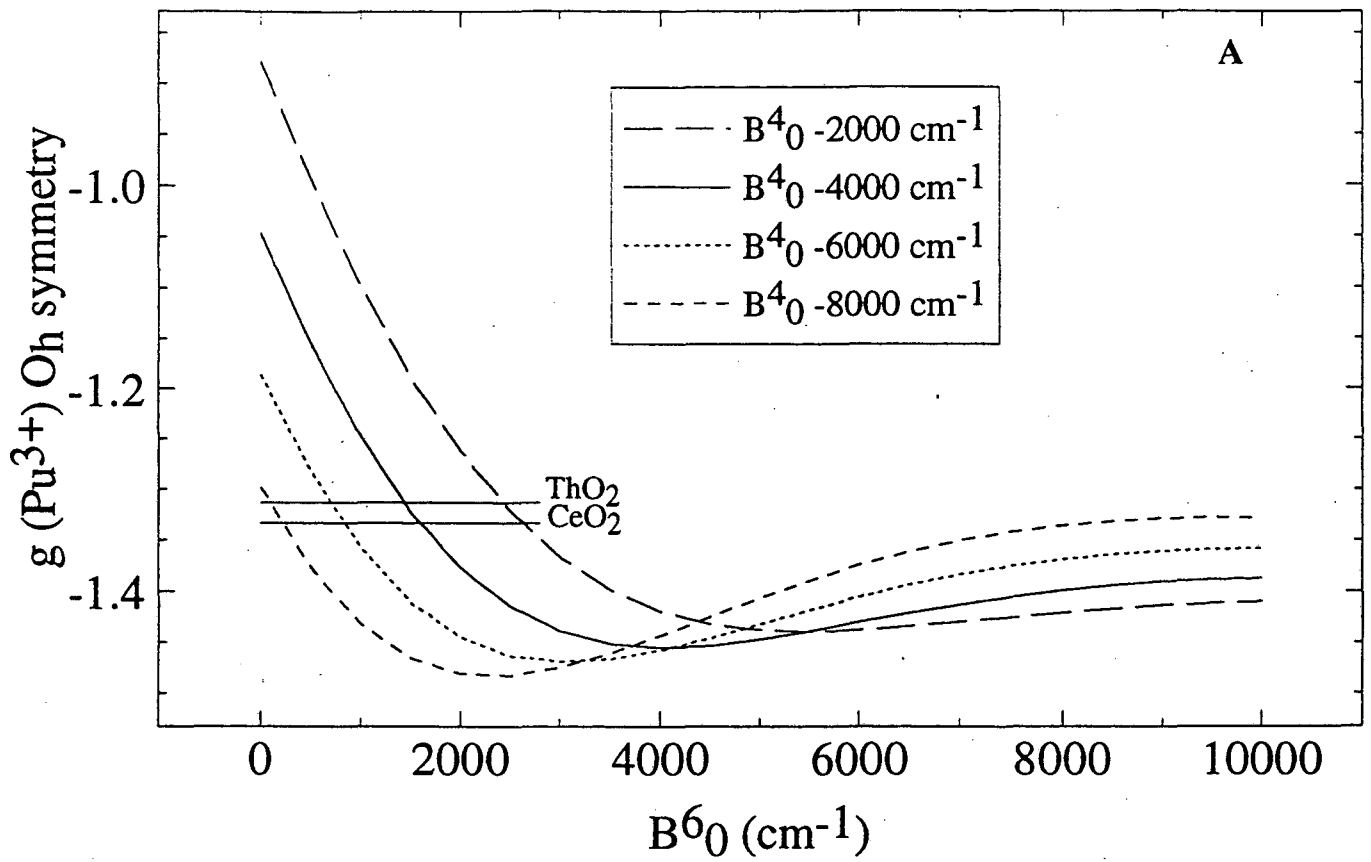


Figure 1
Page 26

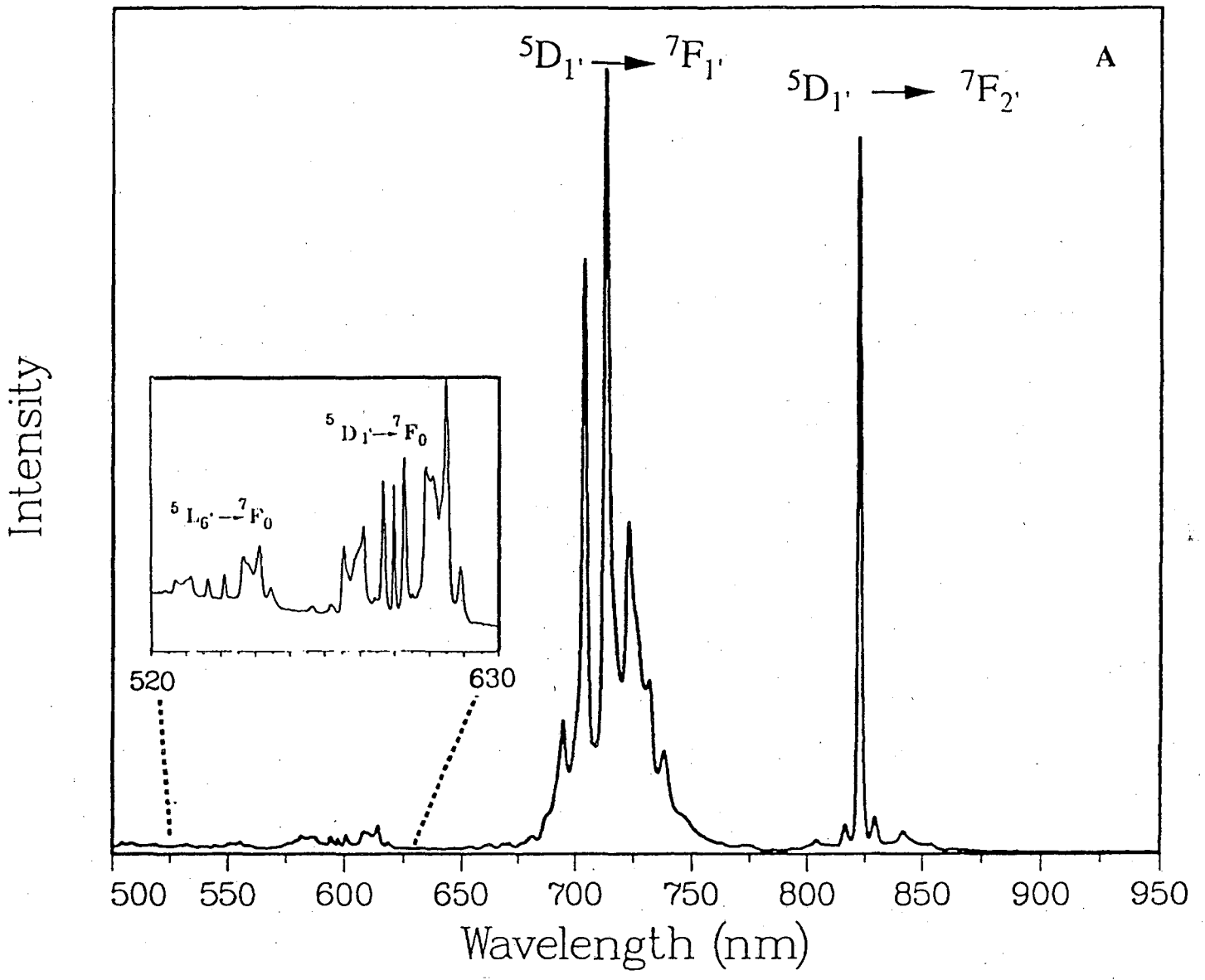


Figure 2A

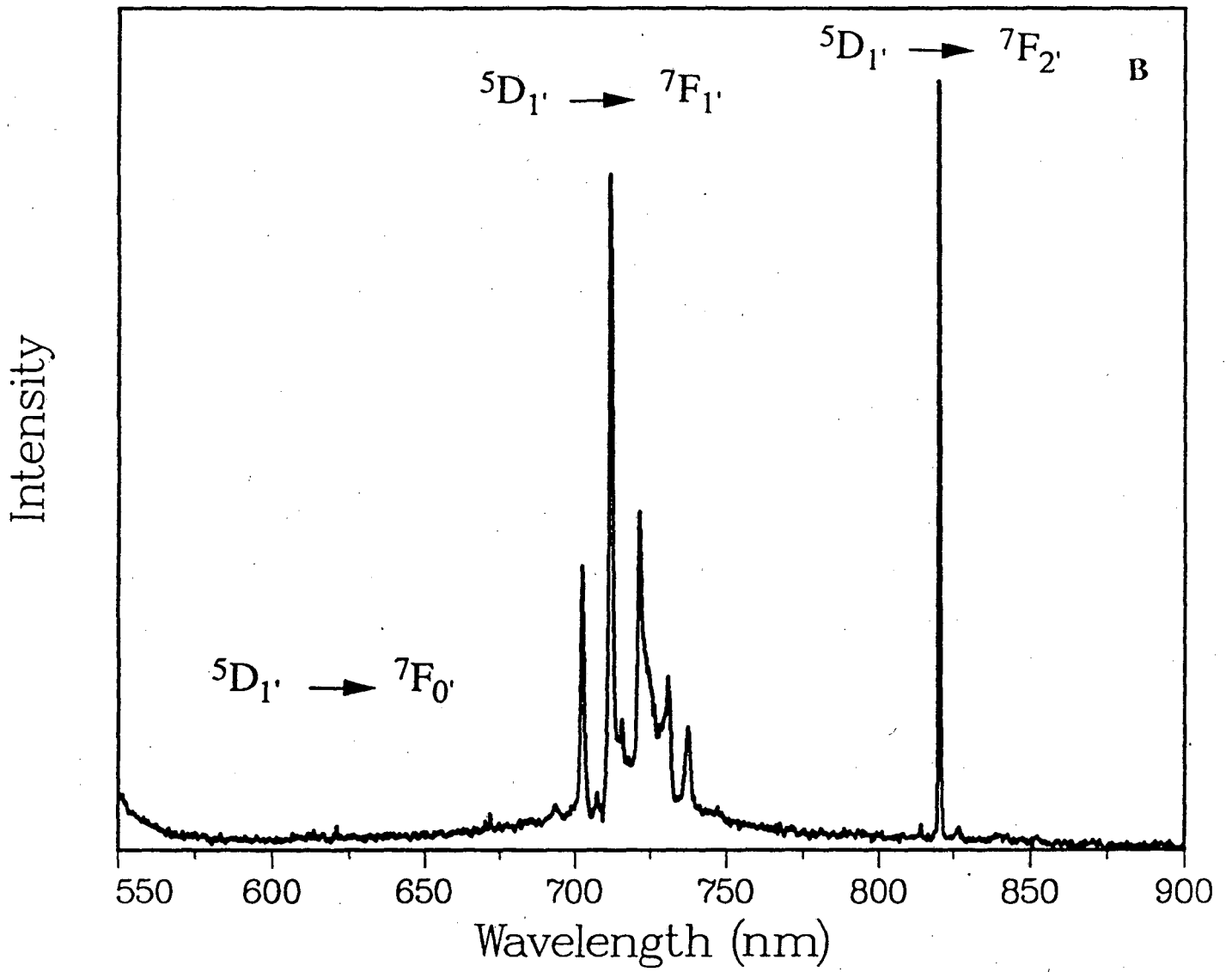


Figure 2B

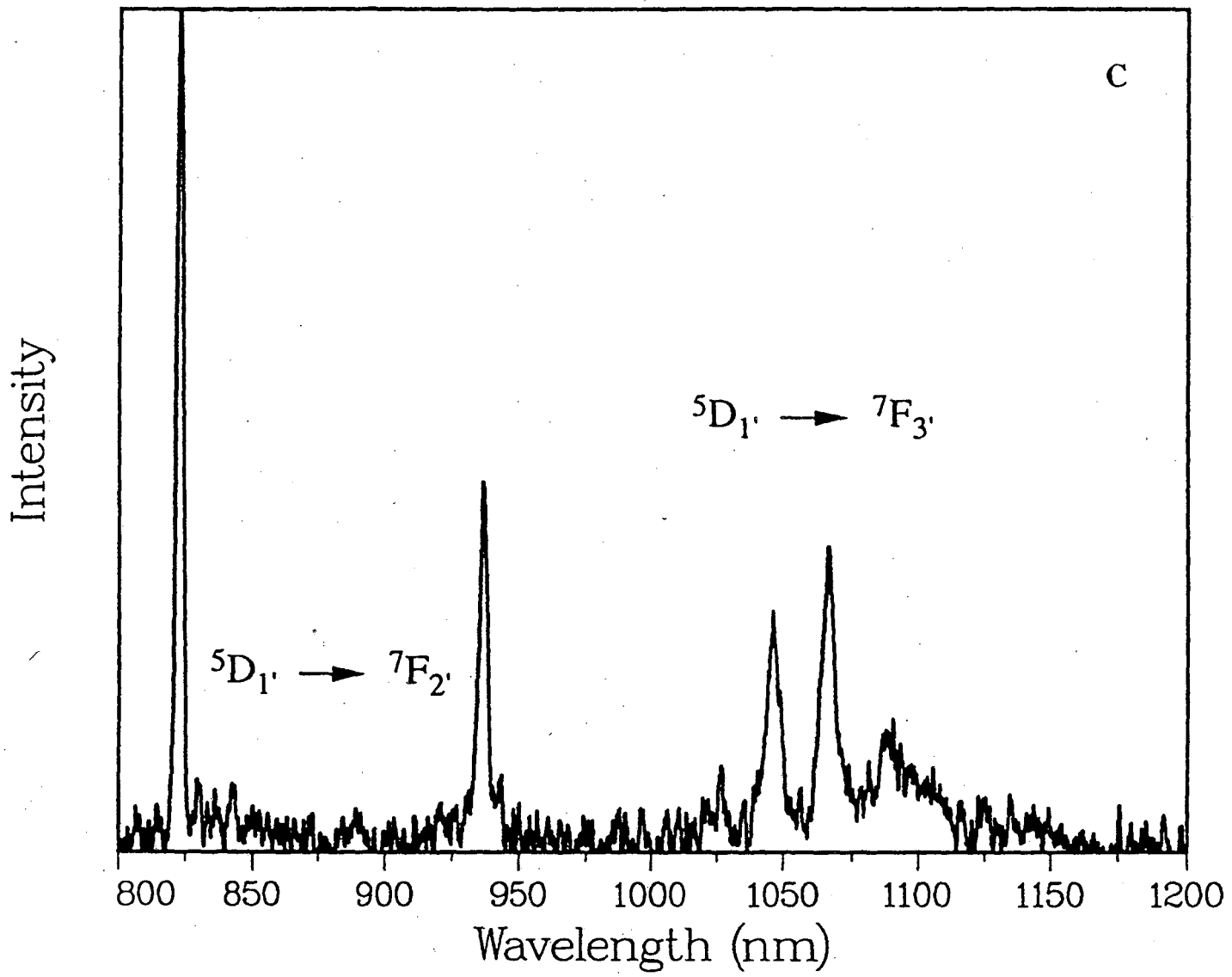


Figure 2C

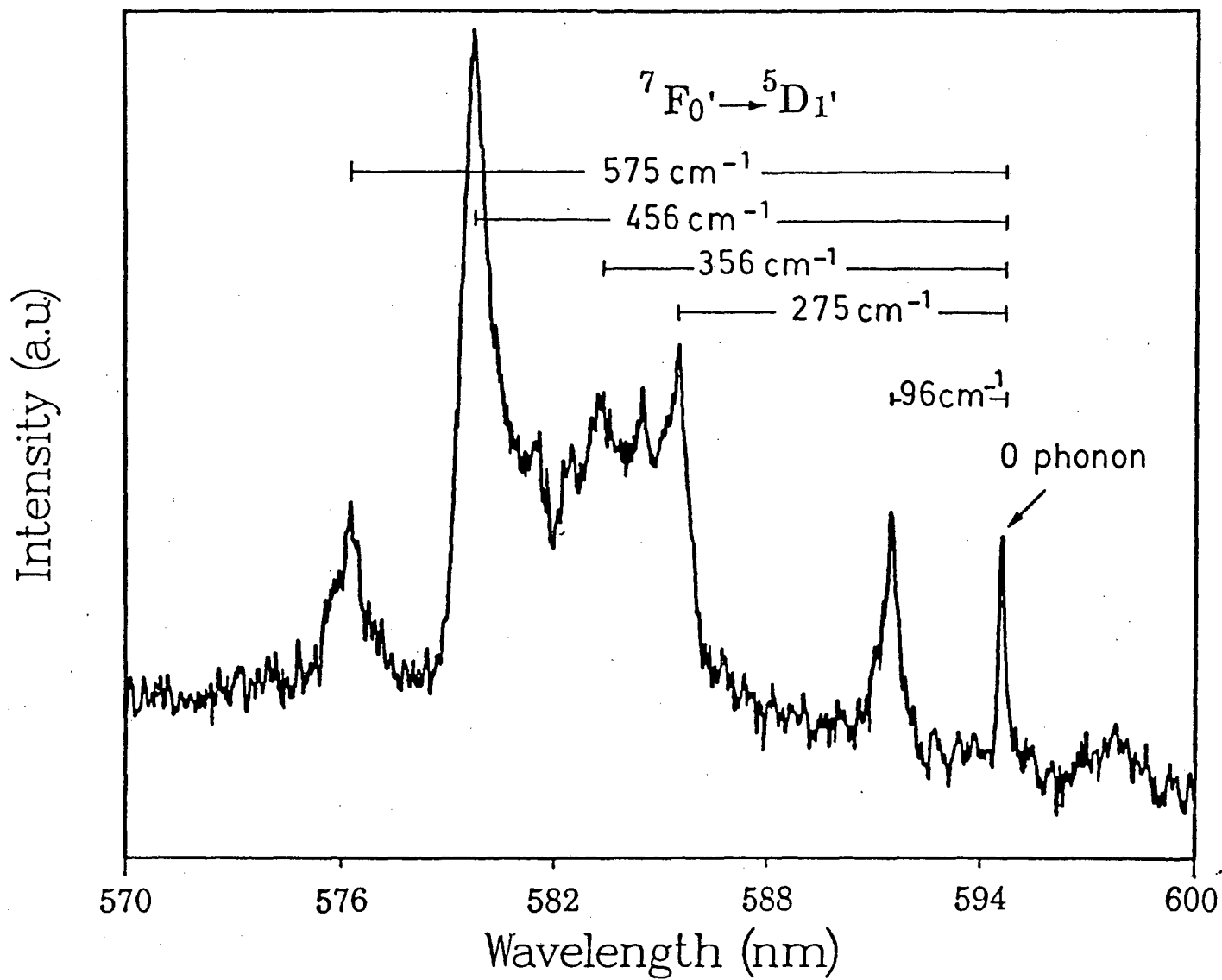


Figure 3

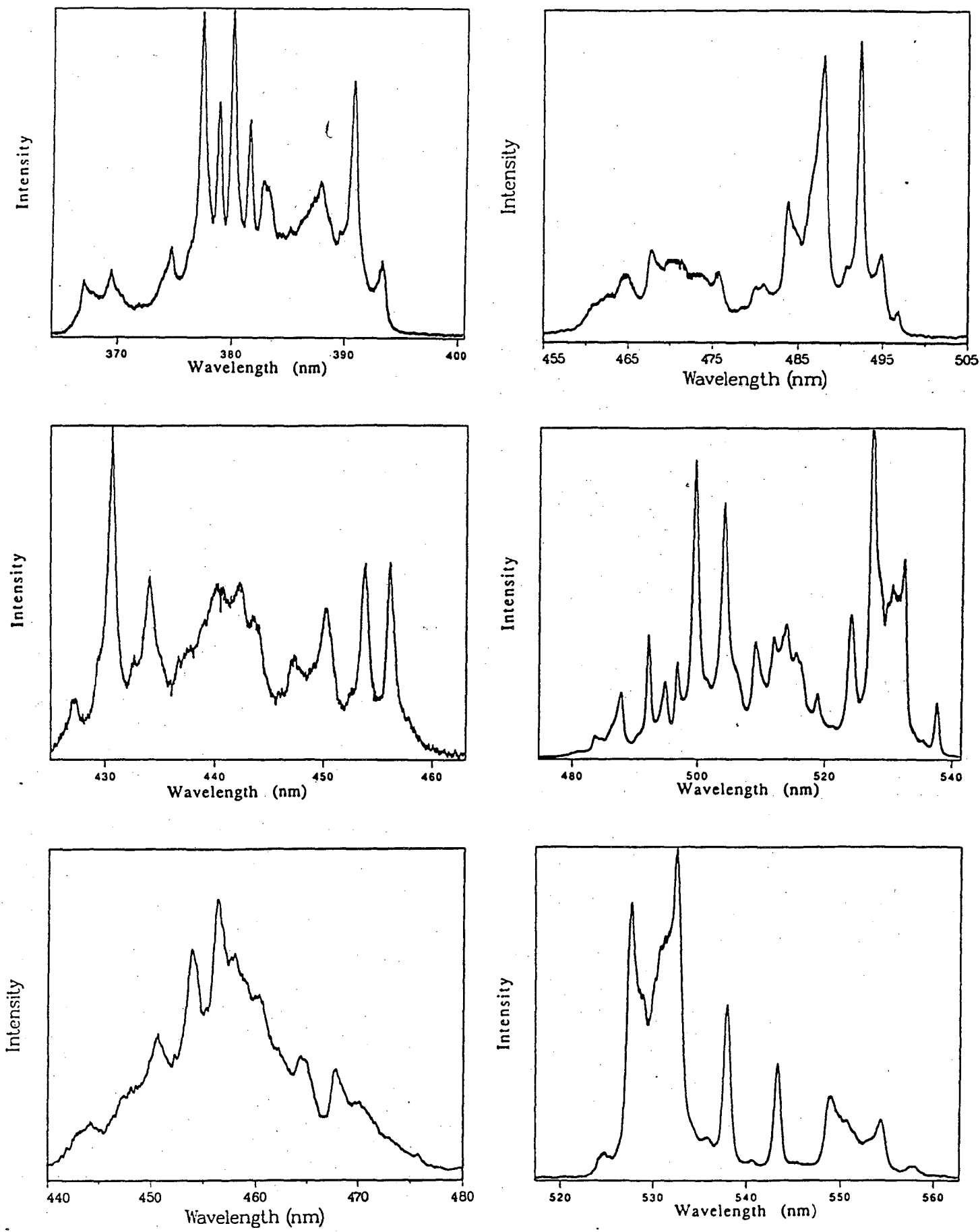


Figure 4

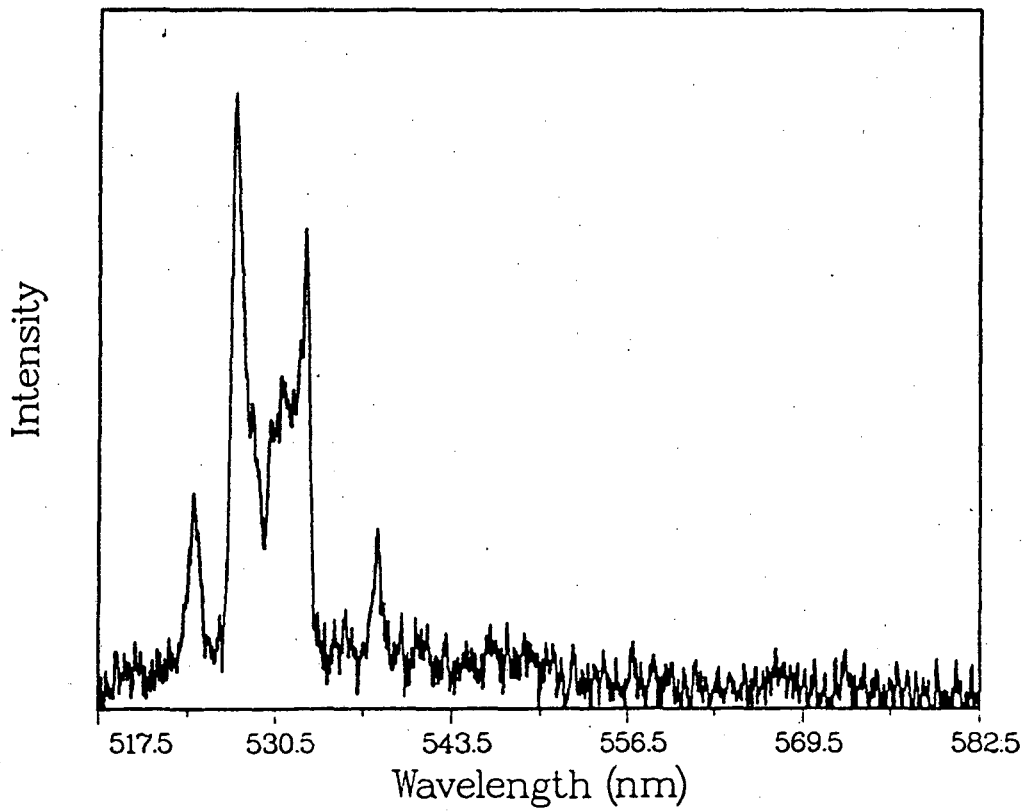
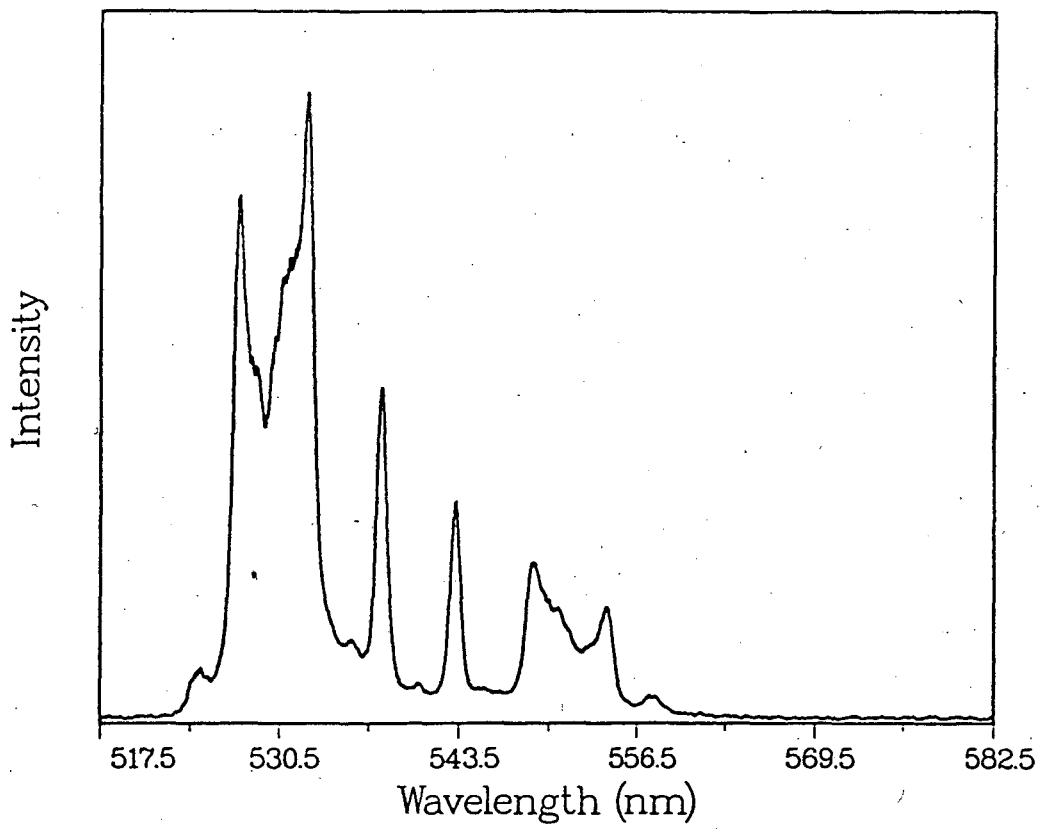


Figure 5

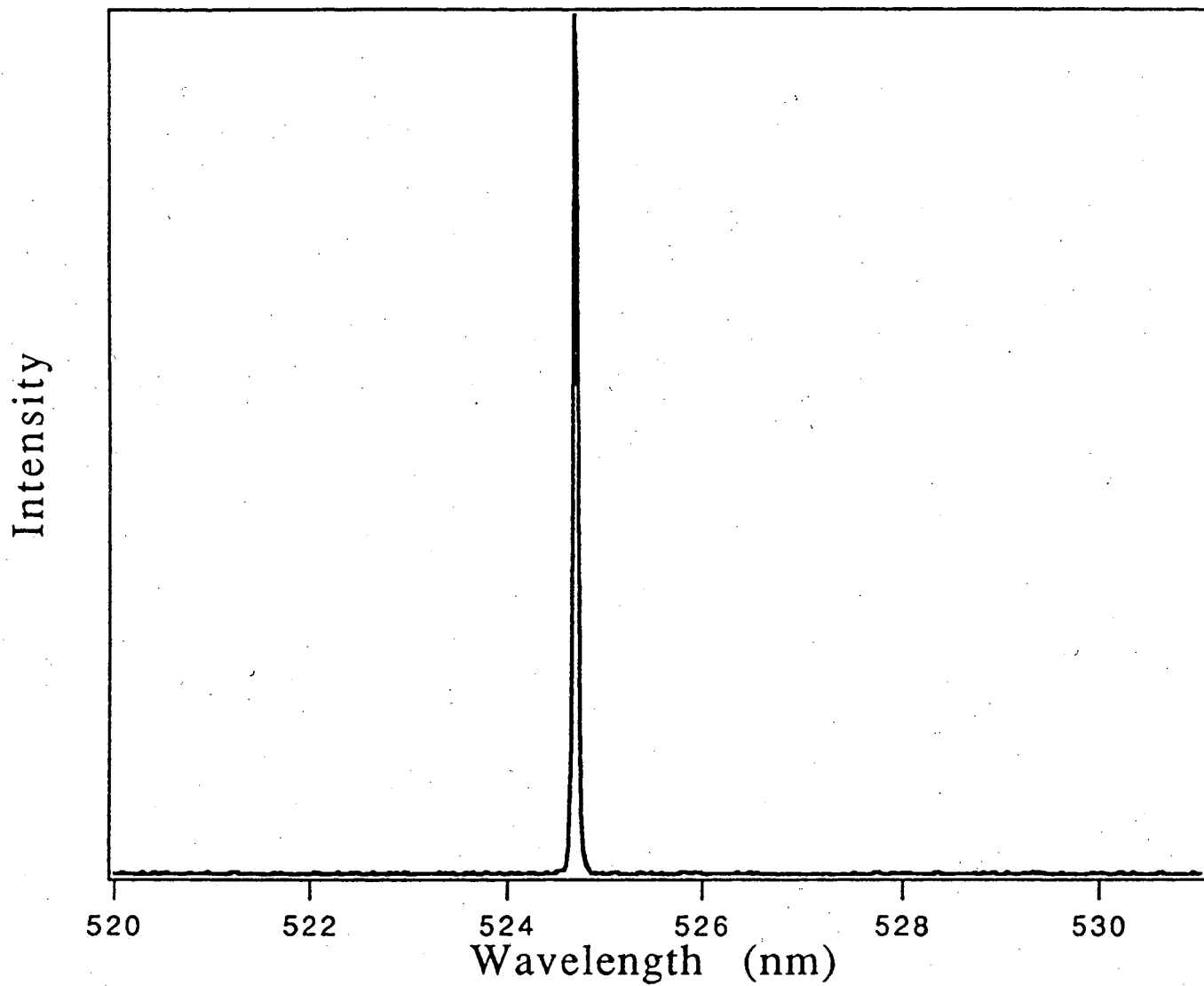


Figure 6

LAWRENCE BERKELEY LABORATORY
UNIVERSITY OF CALIFORNIA
TECHNICAL INFORMATION DEPARTMENT
BERKELEY, CALIFORNIA 94720